The Kinetic Mechanism of Wild-Type and Mutant Mouse Dihydrofolate Reductases†

Joelle Thillet,‡ Joseph A. Adams,§ and Stephen J. Benkovic*,§

Institut Jacques Monod, Universite Paris VII, Place Jussieu, 75251 Paris Cedex 05, Paris, France, and Department of Chemistry, 152 Davey Laboratory, The Pennsylvania State University, University Park, Pennsylvania 16802

Received September 20, 1989; Revised Manuscript Received January 16, 1990

ABSTRACT: A kinetic mechanism is presented for mouse dihydrofolate reductase that predicts all the steady-state parameters and full time-course kinetics. This mechanism was derived from association and dissociation rate constants and pre-steady-state transients by using stopped-flow fluorescence and absorbance measurements. The major features of this kinetic mechanism are as follows: (1) the two native enzyme conformers, E_1 and E_2, bind ligands with varying affinities although only one conformer, E_1, can support catalysis in the forward direction, (2) tetrahydrofolate dissociation is the rate-limiting step under steady-state turnover at low pH, and (3) the pH-independent rate of hydride transfer from NADPH to dihydrofolate is fast (k_{hyd} = 9000 s^{-1}) and favorable (K_{eq} = 100). The overall mechanism is similar in form to the *Escherichia coli* kinetic scheme (Fierke et al., 1987), although several differences are observed: (1) substrates and products predominantly bind the same form of the *E. coli* enzyme, and (2) the hydride transfer rate from NADPH to either folate or dihydrofolate is considerably faster for the mouse enzyme. The role of Glu-30 (Asp-27 in *E. coli*) in mouse DHFR has also been examined by using site-directed mutagenesis as a potential source of these differences. While aspartic acid is strictly conserved in all bacterial DHFRs, glutamic acid is conserved in all known eucaryotes. The two major effects of substituting Asp for Glu-30 in the mouse enzyme are (1) a decreased rate of folate reduction and (2) an increased rate of hydride transfer from NADPH to dihydrofolate. The former effect suggests that the addition of a single methylene group can account, in part, for the species specificity observed for folate reduction.

Dihydrofolate reductase (DHFR)[1] (5,6,7,8-tetrahydrofolate:$NADP^+$ oxidoreductase, EC 1.5.1.3) plays a central metabolic role by catalyzing the NADPH-dependent reduction of dihydrofolate (H_2F) to tetrahydrofolate (H_4F), an essential cofactor in the synthesis of thymidylate, purines, and several amino acids. Consequently, DHFR is a target enzyme for antifolate drugs such as methotrexate (antineoplastic drug) and trimethoprim (antibacterial drug).

Detailed structural studies including X-ray crystallography of DHFR and some of its complexes has been accomplished for the enzyme from *Lactobacillus casei* (Matthews et al., 1985), *Escherichia coli* (Bolin et al., 1982), and chicken liver (Volz et al., 1982). The refined structures of mouse L1210 DHFR complexed with NADPH and either TMP or MTX have also been solved (Stammers et al., 1987). In comparison to bacterial DHFRs, the primary sequence homology among vertebrate enzymes is very high (e.g., 100% of active-site residues between mouse and human DHFRs). Comparison of all these structures reveals that bacterial and vertebrate reductases, although showing little primary sequence homology, possess an active site constructed of ca. 50% homology (avian versus *E. coli*). Despite these congruences, bacterial and vertebrate DHFRs differ in several key properties. For example, some of the inhibitors show a high species selectivity. In addition, the vertebrate enzymes can efficiently reduce folic acid while the bacterial ones have a negligible activity.

Detailed kinetic studies have been previously performed on the *E. coli* (Fierke et al., 1987) and *L. casei* (Andrews et al., 1989) DHFRs, and complete kinetic mechanisms have been established from these studies. Although the crystallographic structures of several vertebrate DHFRs have been solved, there is no coherent kinetic scheme for this class of enzymes that can be used as a background to determine the effects of single amino acid changes for comparison with the bacterial sources. The results reported in this present study describe a complete kinetic scheme for wild-type mouse DHFR. In addition the active-site proton donor, Glu-30, has been replaced with aspartic acid by site-directed mutagenesis. This change was selected since aspartic acid and glutamic acid are strictly conserved in bacterial and vertebrate sources, respectively, and may encompass some of the primary differences between the two classes.

Materials and Methods

Materials. 7,8-Dihydrofolate was prepared from folic acid by the method of Blakley (1960), and (6*S*)-tetrahydrofolate was prepared from H_2F by using *E. coli* dihydrofolate reductase (Matthews & Huennekens, 1960) and purified on a DE-52 resin eluting with a triethylammonium bicarbonate gradient (Curthoys et al., 1972). [4′(*R*)-^{2}H]NADPH (NADPD) and TNADPH were prepared by using *Leuconostoc mesenteroides* alcohol dehydrogenase (Viola et al., 1979) obtained from Research Plus, Inc., and purified on a Mono Q column using a NaCl gradient. Excess NaCl was removed from the purified NADPD by a Bio-Gel P-2 desalting column (Howell et al., 1987). The concentrations of ligands

† This work was supported by NIH Grant GM24129 (to S.J.B.) and by grants from the French Ministere de la Recherche et Technologie and from the Centre National de la Recherche Scientifique to R. Pictet.

* To whom correspondence should be addressed.

‡ Universite Paris.

§ The Pennsylvania State University.

[1] Abbreviations: DHFR, dihydrofolate reductase; mDHFR, wild-type mouse DHFR; E30D, Glu30 → Asp; H_2F, 7,8-dihydrofolate; H_4F, 5,6,7,8-tetrahydrofolate; MTX, methotrexate; TMP, trimethoprim; DAM, 2,4-diamino-6,7-dimethylpteridine; TNADPH, thionicotinamide adenine dinucleotide phosphate, reduced; NADPH, nicotinamide adenine dinucleotide phosphate, reduced; $NADP^+$, nicotinamide adenine dinucleotide phosphate.

0006-2960/90/0429-5195$02.50/0

were determined spectrophometrically by using the following extinction coefficients: H_2F, 28 000 M^{-1} at 282 nm, pH 7.2 (Dawson et al., 1969); folic acid, 27 600 M^{-1} at 282 nm, pH 7.0 (Rabinowitz, 1960); H_4F, 28 000 M^{-1} at 297 nm, pH 7.5 (Kallen & Jencks, 1966); MTX, 22 100 M^{-1} at 302 nm in 0.1 N KOH (Seeger, et al., 1949); DAM, 6900 M^{-1} at 346 nm, pH 6.0 (Brown & Jacobsen, 1961); NADPH, 6220 M^{-1} at 340 nm, pH 7.5; $NADP^+$, 18 000 M^{-1} at 259 nm; TNADPH, 11 300 M^{-1} at 395 nm. NADPH and $NADP^+$ were purchased from Sigma and used without further purification. The concentration of H_2F was also determined by enzymatic turnover with mDHFR.

Enzymes. The E30D mutant was made by oligonucleotide-directed mutagenesis and the mutant DNA transferred in the expression vector as previously described (Thillet et al., 1988). The purification of both wild type and mutant were also performed as described (Thillet et al., 1988) without the methotrexate affinity resin. The modifications include the following: (1) *E. coli* strain HB101 was used as the recipient for both wild-type and mutant plasmids, (2) T-broth medium was used, which doubles the specific activity by increasing the plasmid copy number, and (3) the ammonium sulfate precipitation was always between 55 and 80% saturation. In both cases the enzymes were shown to be homogeneous by SDS–PAGE. The enzyme concentrations were determined by MTX titration.

Kinetics. All kinetic measurements were performed at 25 °C in buffers containing 50 mM 2-(*N*-morpholino)ethanesulfonic acid, 25 mM tris(hydroxymethyl)aminomethane, 25 mM ethanolamine, and 0.8 M sodium chloride (MTEN buffer). The buffers contained 1 mM dithiothreitol and were purged with argon when H_4F was used.

Steady-State Kinetics. Steady-state kinetics were performed on a Cary 219 UV–vis spectrophotometer or on the stopped-flow instrument in the absorbance mode. The molar absorbance change used in the former case was 11 800 M^{-1} (Stone & Morrison, 1983) and 3000 M^{-1} in the latter case. The stopped-flow apparatus was used to measure steady-state turnover only when very high NADPH concentrations were needed (>200 μM). Typically the enzyme was preincubated with NADPH and the reaction was initiated with H_2F. In the reverse direction, the enzyme was preincubated with H_4F and the reaction initiated with $NADP^+$. The values for V and V/K at each specific pH were fit to the equation

$$C = C^{max}[H]/([H] + K_a) \quad (1)$$

where C^{max} and C are the pH-independent and -dependent values for either V or V/K. The inhibition constant of DAM, $K_{i,obs}$, was obtained by plotting $1/V$ versus the inhibitor concentration (Segel, 1975). These data were then fit to the equation

$$K_{i,obs} = K_{i,app}/(1 + [H_2F]/K_M) \quad (2)$$

The values of $K_{i,app}$ were then fit to the equation

$$K_{i,app} = K_1(1 + [H]/K_b)(1 + K_a/[H]) \quad (3)$$

where K_1 is the pH-independent dissociation constant of DAM and K_a and K_b are the acid dissociation constants of the free enzyme and DAM, respectively.

Equilibrium Dissociation Constants. The emission spectra of enzymes, ligands, and their complexes were measured on a SLM8000 spectrofluorometer interfaced to an IBM-PC computer. Equilibrium dissociation constants for DHFR and ligands in all binary complexes were determined by titrating the change in enzyme fluorescence that accompanies complex formation. Titrations were typically carried out by serial addition of concentrated ligand to a buffered solution contained in a quartz curvette. Correction for ligand absorbance was calculated from parallel titrations in which enzyme was replaced by a quantity of tryptophan with a fluorescence intensity equal to that of the enzyme. The results were fitted as previously described (Taira & Benkovic, 1988) to determine K_D values.

Transient Kinetics. Association and dissociation rate constants and pre-steady-state kinetic data were obtained with a stopped-flow apparatus built in the laboratory of Johnson (Johnson, 1986) operating in either a fluorescence or transmittance mode, with a 1.6-ms dead time, a 2-mm path length, and a thermostated sample cell. Complex formation and ligand trapping studies were followed by excitation at 290 nm and by monitoring either the quenching of the intrinsic protein fluorescence at 340 nm or the enhancement of coenzyme fluorescence by energy transfer at 450 nm (Fierke et al., 1987). For pre-steady-state kinetics, the reaction was monitored by either fluorescence energy transfer or transmittance. In the latter case, 340 nm was used and the transmittance was later converted to absorbance. Molar absorbance and fluorescence changes were determined as described (Fierke et al., 1987).

In most experiments the average of at least six runs was used for data analysis. The data were collected over a given time interval by a computer and analyzed by an iterative, nonlinear least-squares fit computer program using a modification of the method of moments (Dyson & Isenberg, 1971; Johnson, 1986). Kinetic data were analyzed with either a single exponential, a double exponential, or a single exponential followed by a linear rate. The data were then transferred to a Vax microcomputer where a fit to more complicated models was tested by using the computer program KINSIM (Barshop et al., 1983).

Results

Steady-State Kinetics. The steady-state kinetic parameters V and K_m have been determined by varying $[H_2F]$ at fixed [NADPH] as well as fixed $[H_2F]$ and varying [NADPH]. In the former case the double-reciprocal plots are linear over all concentrations of H_2F. However, for both wild-type and mutant enzymes these plots show significant curvature under conditions of fixed $[H_2F]$ (50 μM). Since two distinct V's and K_m's are approached, a modified form of the Michaelis–Menten equation was used to analyze all the steady-state kinetics:

$$v = V_1[S]/(K_1 + [S]) + V^*[S]/(K_2 + [S]) \quad (4)$$

where [S] is the concentration of NADPH, V_1 and K_1 are the respective maximum velocity and apparent dissociation constant approached at low NADPH, and V_2 ($V^* + V_1$) and K_2 are the respective maximum velocity and apparent dissociation constant approached at high NADPH. Under conditions of both low and high coenzyme concentration, V and V/K increase as the pH decreases until a plateau is reached at low pH, suggesting that the protonation of a residue on the enzyme is important for determining the maximum velocity. The pH-independent values for V and V/K under these two conditions and the pK_a's associated with them are listed in Table I for both wild-type and mutant enzymes. The observed isotope effects on V and V/K with [4′(*R*)-^{2}H]NADPH (NADPD) have also been determined at a number of pH values and are listed in Table I. The rate of the reverse reaction (net conversion of H_4F and $NADP^+$ to form H_2F and NADPH) was measured from the increase in absorbance at 340 nm in a reaction mixture containing 280 μM H_4F, 840 μM $NADP^+$, and 50 nM enzyme at pH 10. The observed rate

Table I: Steady-State Parameters for Folate and Dihydrofolate Reduction by mDHFR[a]

	wild type	E30D
50 μM Dihydrofolate, Varying [NADPH]		
V_1 (s^{-1})	17 ± 1	5 ± 1 (pH 7)
pK_a (V_1)	9.46 ± 0.05	
V_1/K (μM^{-1} s^{-1})	3.63 ± 0.01	2 ± 0.4
pK_a (V_1/K)	9.38 ± 0.05	
V_2 (s^{-1})	36 ± 2 (pH 7)	63 ± 3
pK_a (V_2)	9.15 ± 0.07	8.24 ± 0.02
V_2/K (μM^{-1} s^{-1})	0.6 ± 0.1 (pH 7)	0.6 ± 0.1
pK_a (V_2/K)		8.84 ± 0.07
$^HV_1/^DV_1$	1.0 ± 0.12 (pH 8.5)	1.18 ± 0.12 (pH 7)
$^HV_1/^DV_1$	3.3 ± 0.25 (pH 10)	3.0 ± 0.15 (pH 9.5)
Varying [Folate], 100 μM NADPH		
V (s^{-1})	0.44 ± 0.03 (pH 6)	0.060 ± 0.002
V/K (μM^{-1} s^{-1})	0.044 ± 0.01 (pH 6)	0.020 ± 0.004
$^HV/^DV$	3.0 ± 0.1 (pH 6)	4.2 ± 0.05 (pH 5.7)
$^HV/^DV$	3.0 ± 0.1 (pH 7)	4.2 ± 0.03 (pH 6.5)

[a] MTEN buffer, 25 °C.

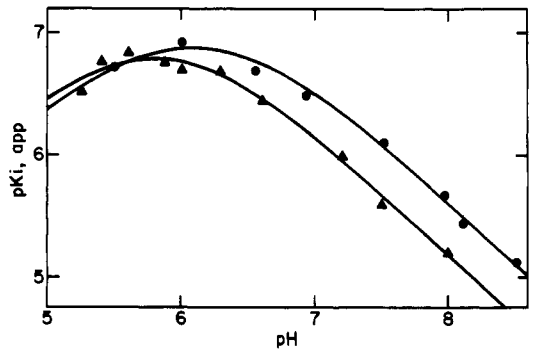

FIGURE 1: Variation with pH of the $pK_{i,app}$ [$-\log K_{i,app}$ (M)] for inhibition of mDHFR (●) and D30E (▲) by DAM. The solid lines are theoretical fits to eq 3 where pK_a = 6.40 ± 0.05 for mDHFR and 6.0 ± 0.10 for E30D, pK_I = 7.2 ± 0.20 for mDHFR and 7.33 ± 0.04 for E30D, and pK_B was fixed to 5.7 for E30D.

of these reactions was unaffected by either doubling the substrate concentrations or lowering the pH to 9. Under these conditions a value of 7.2 ± 0.9 s^{-1} for k_{cat} for the wild-type enzyme was obtained.

Steady-state parameters have also been measured with varying concentrations of folic acid (1–50 μM) at 100 μM NADPH as a function of pH for wild-type and mutant enzymes. However, in contrast to the H_2F reaction, there is no evidence for a plateau in V. Consequently, values for V and V/K given in Table I are not pH independent. Nevertheless, plots of log V (folate) versus pH follow a slope close to −1 over the entire pH range of 5–8. The observed deuterium isotope effect with NADPD has also been determined at all pH values studied and was found to be >3 for both wild type and mutant (Table I).

pH-Dependent Inhibition by DAM. The intrinsic pK_a's of the wild-type and mutant enzymes were determined from the inhibition caused by the competitive inhibitor 2,4-diamino-6,7-dimethylpteridine (DAM). The variation with pH of the inhibition by DAM yielded a bell-shaped curve for both enzymes. These are illustrated in Figure 1. For wild-type DHFR, two pK_a values of 5.75 ± 0.1 and 6.40 ± 0.05 were fit. The lower value corresponds to the pK_a of the free DAM (Stone & Morrison, 1983) while the higher one corresponds to the pK_a of a residue on the enzyme. It has been shown that the active-site proton donor in the *E. coli* DHFR is Asp-27 (Howell et al., 1986). By analogy, Glu-30 of mouse DHFR is likely the residue involved in this protonation. For the mutant, the higher pK_a (6.0 ± 0.1) corresponds to Asp-30.

Table II: Thermodynamic Dissociation Constants[a]

	K_d (μM)	
	wild type	E30D
NADPH	1.85 ± 0.16	0.89 ± 0.15
$NADP^+$	3.71 ± 0.22	28 ± 5
folate	1.66 ± 0.07	0.69 ± 0.04
H_2F	0.81 ± 0.07[b]	0.28 ± 0.05
H_4F	0.2 ± 0.01	0.22 ± 0.01

[a] Values were recorded at pH 7, MTEN buffer, 25 °C. [b] Identical at pH 9.

Table III: Kinetic Binding Constants for mDHFR at pH 7: Relaxation Method

ligand	enzyme species	k_{on} (μM^{-1} s^{-1})	k_{off} (s^{-1})	k_{off}/k_{on}
NADPH	E	2.8 ± 0.1	2.4 ± 0.4	0.85
	E-H_4F	1.0 ± 0.4	26 ± 15	
	E-MTX	2.7 ± 0.1	2.2 ± 0.6	
$NADP^+$	E	6.8 ± 0.2	13 ± 5	1.91
	E-H_4F	9 ± 0.4	21 ± 6	
	E-H_2F	2 ± 0.15	7.3 ± 0.9	
H_2F	E	33 ± 5	21 ± 6	0.63
H_4F	E	33 ± 2	14 ± 4	0.42
	$E-N^+$	18 ± 2	18 ± 6	
	E-NH	5 ± 3	34 ± 8	

Scheme I

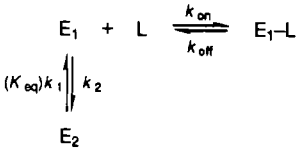

Equilibrium Binding of Ligands. Excitation of wild-type mouse DHFR at 290 nm leads to fluorescence emission that has a maximum value at 325 nm. The thermodynamic dissociation constants (K_d) of ligands and free enzyme were measured by using the ligand-dependent fluorescence quenching upon formation of the binary complex. The observed fluorescence intensity was measured as a function of added ligand and fit to a quadratic solution as previously outlined (Taira & Benkovic, 1988). K_d values for ligands to both wild-type and mutant DHFRs are presented in Table II.

Kinetic Binding of Ligands—Relaxation. Stopped-flow quenching of the intrinsic enzyme fluorescence has been used to measure the association and dissociation rate constants of ligands to DHFR (Dunn & King, 1980; Cayley et al., 1981). In the formation of binary complexes of DHFR the observed rate (k_{obs}) increases linearly with ligand concentration when [L] > [E]. Under these pseudo-first-order reaction conditions, $k_{obs} = k_{on}[L] + k_{off}$, where k_{on} and k_{off} are the association and dissociation rate constants, respectively. Thus, a linear plot of k_{obs} versus [L] yields k_{on} from the slope and k_{off} from the k_{obs} intercept. The association and dissociation rate constants for some ligands to free and binary complexes of wild-type mouse DHFR are shown in Table III.

In the formation of the E–NADPH complex, two exponential rates, one ligand dependent and the other ligand independent, were observed. According to Cayley et al. (1981), this observation is consistent with Scheme I, in which there are two slowly interconverting forms of the enzyme, E_1 and E_2. In this scheme the rapid phase is ligand dependent and corresponds to the binding of L and E_1 while the slow phase is ligand independent and corresponds to the interconversion of E_2 to E_1. The rate of interconversion of E_2 to E_1 (k_1) can be obtained from the slow phase while the equilibrium constant (K_{eq}) can be obtained from the ratio of the amplitudes of the

Table IV: Dissociation Rate Constants for mDHFR at pH 7: Competition Method

ligand	enzyme species	trapping ligand	k_{off} (s^{-1}) wild type	k_{off} (s^{-1}) E30D
NADPH	E–NH	$NADP^+$	2.8 ± 0.3	7 ± 1
$NADP^+$	$E–N^+$	NADPH	90 ± 10[a]	90 ± 5[a]
			0.053 ± 0.01[b]	0.043 ± 0.01[b]
	$E–H_4F–N^+$	NADPH	440 ± 40[a]	
			0.15 ± 0.05[b]	
H_2F	$E–H_2F$	MTX	20 ± 2	
H_4F	$E–H_4F$	MTX	15 ± 0.5	9 ± 1
	$E–N^+–H_4F$	MTX	20 ± 1	17 ± 1

[a] Values represent the dissociation rate constants for $NADP^+$ from either binary or ternary complexes of E_1. [b] Values correspond to the nondissociative protein isomerization $E_2 \rightarrow E_1$.

fast and slow phases. For the wild-type and mutant enzymes $K_{eq} = 1.0 \pm 0.1$ when NADPH was used. For the wild type, k_1 was found to be 0.048 ± 0.002 s^{-1}. In addition, no ligand dependence in the slow phase was observed. This is supportive of the above binding mechanism for NADPH. The K_d for NADPH can be related to k_{on} and k_{off} by eq 5. Since K_{eq}

$$K_d = k_{off}/k_{on}(1 + 1/K_{eq}) \quad (5)$$

= 1 for the wild-type enzyme, the predicted K_d is twice the ratio of k_{off}/k_{on}. The agreement of the thermodynamic (Table II) and kinetic (Table III) data supports Scheme I for NADPH binding and, within error, H_2F association. In contrast, the binding of H_4F does not fit the above criterion, since the ratio of k_{off}/k_{on} was not close in value to the K_d. Possible reasons for these differences will be cited under Discussion. The binding of $NADP^+$, although ostensibly in agreement, is more complex as revealed below.

Dissociation Rate Constants—Competition. The dissociation rate constants of ligands to DHFR can also be measured by a competition method (Dunn et al., 1978; Birdsall et al., 1980). In this technique, the preequilibrated enzyme–ligand complex ($E–L_1$) is mixed with a large excess of a second ligand (L_2) that competes for the same binding site. The observed change in fluorescence reflects the release of L_1 from the original enzyme complex, $E–L_1$, and formation of the new complex, $E–L_2$. This process is described in Scheme II.

Scheme II

$$E–L_1 \underset{k_1}{\overset{k_{-1}}{\rightleftharpoons}} E + L_1$$

$$E + L_2 \underset{k_{-2}}{\overset{k_2}{\rightleftharpoons}} E–L_2$$

When $k_1[L] \ll k_2[L_2] \gg k_{-1}$ and $k_2[L_2]/k_{-2} \gg k_1[L_1]/k_{-1}$, k_{obs} for this reaction is equal to the dissociation rate constant for L_1, k_{-1}. The validity of this measurement is checked by showing that k_{obs} is independent of the concentration of L_2. The dissociation rate constants for several ligands to both binary and ternary complexes of wild-type and mutant DHFRs are shown in Table IV. The values reported for NADPH, H_2F, and H_4F are consistent with dissociation rate constants determined by relaxation (Table III). This observation indicates that the competition method is a valid alternative to measuring off rates of ligands. For $NADP^+$, the observed dissociation is biphasic and inconsistent with the relaxation data. Both the rates (Table IV) and relative amplitudes (ratio of fast to slow phases is 1 for $E–NADP^+$ and 7 for $E–NADP^+–H_4F$) for these two transients are independent of the concentrations of $NADP^+$ and NADPH. The rapid phases have been assigned to the dissociation rate constant for $NADP^+$ from $E_1–NADP^+$ or $E_1–NADP^+–H_4F$ (see Discussion).

Pre-Steady-State Kinetics. The observed rate of hydride transfer from NADPH to H_2F was measured from pre-steady-state transients. A rapid burst of product formation was observed by monitoring changes in either absorbance or fluorescence energy transfer (Fierke et al., 1987). Typically, 10 μM DHFR was preincubated with 100 μM NADPH or NADPD before 100 μM H_2F was rapidly added. Original experiments were performed in MTEN buffer containing 0.1 M NaCl. Under these conditions the pre-steady-state burst as measured by absorbance corresponded to formation of 3.8 ± 0.2 mol of product/mol of enzyme at pH 7. Furthermore, the burst as measured by energy transfer could be characterized as biphasic followed by a linear steady-state rate. The faster phase varied with pH and presented an observed deuterium isotope effect, although this phase was difficult to measure due to its low amplitude and fast rate. In contrast, the slow phase (30 s^{-1}) was independent of pH and no isotope effect was observed (data not shown). These results demonstrated that the burst under these conditions was complicated.

In order to simplify the analysis of the hydride transfer step, the salt concentration of MTEN was varied from 0.1 to 0.8 M NaCl. Under these conditions the burst amplitudes were measured by absorbance. These results revealed that the number of enzyme equivalents decreased as the salt concentration increased until the total amplitude was slightly less than 1 at 0.8 M NaCl. Also, suppressing the isotope-insensitive step by added salt resulted in pre-steady-state transients as measured by fluorescence energy transfer that fit well to a single exponential followed by a linear rate. Consequently, 0.8 M NaCl was chosen to study all pre-steady-state as well as steady-state and binding kinetics. All the pre-steady-state transients were fit either to a single exponential followed by a linear rate or more precisely by the kinetic simulation program KINSIM according to Scheme III. In this scheme, k_{on} was measured under single-turnover conditions (Fierke et al., 1987) and the value of k_{off} (12 s^{-1}) was equated to that measured for dissociation of H_2F from the mock ternary complex, E–TNADPH–H_2F (see Discussion). The dissociation of $NADP^+$ from the ternary complex, $E–N–H_4F$ (k_N) was taken from Table IV, while that of H_4F from the ternary $E–NH–H_4F$ complex (k_T) was indirectly measured from steady-state simulation using KINSIM (see Discussion). The binding of NADPH to $E–H_4F$ is included in k_T.

Scheme III

$$E–NH + H_2F \underset{k_{off}}{\overset{k_{on}}{\rightleftharpoons}} E–NH–H_2F \underset{k_{-hyd}}{\overset{k_{hyd}}{\rightleftharpoons}} E–N–H_4F \xrightarrow{k_N}$$

$$E–H_4F \xrightarrow{k_T} E–NH$$

Figure 2 shows a typical pre-steady-state transient for wild-type mouse DHFR at pH 7.5. Fitting the data to Scheme III gave a value of 540 ± 40 s^{-1} for the forward hydride transfer rate when the enzyme was preequilibrated with NADPH. Alternatively, the rate of hydride transfer was 180 ± 20 s^{-1} when NADPD was preequilibrated. Thus the observed burst at pH 7.5 is due to the forward hydride step, as evidenced by the large primary isotope effect ($k_{hyd}[H]/k_{hyd}[D] = 3.0 \pm 0.2$). This effect on the pre-steady-state burst was also present at high pH (data not shown). However, as the pH was decreased below 7.5 the observed burst rate of 540 s^{-1} had no isotope effect (data not shown). It is unlikely that this isotope-insensitive phase is due to any conformational change that occurs prior to chemistry, since such a step would be manifest at all pH values. Since the rate of this burst was equivalent to the dissociation rate constant for $NADP^+$ from the ternary $E–N–H_4F$ complex (Table IV), it was concluded

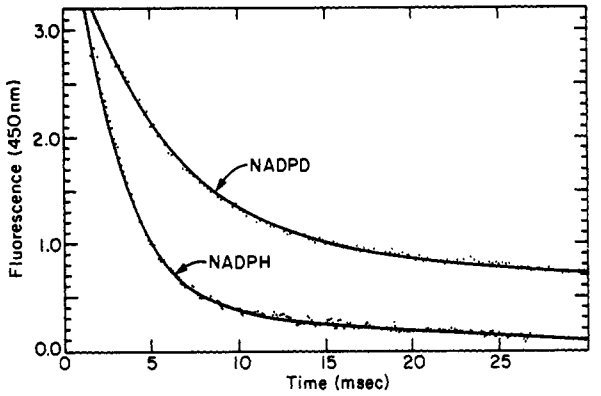

FIGURE 2: Measurement of the pre-steady-state burst for mDHFR by stopped-flow fluorescence energy transfer. The enzyme is preincubated with either NADPH or [4'(*R*)-^{2}H]NADPD and the reaction is initiated with H_2F. Final conditions are 10 μM mDHFR, 50 μM NADPH(D), 50 μM H_2F, pH 7.5, and 25 °C. The lines drawn through both transients are KINSIM computer fits to Scheme III.

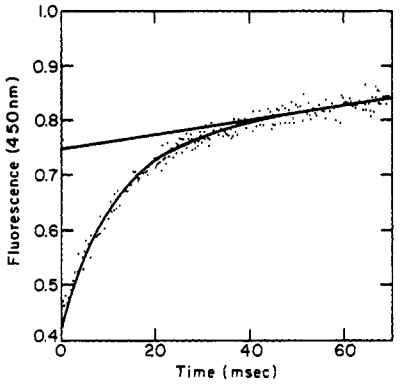

FIGURE 3: Measurement of the pre-steady-state burst for mDHFR in the reverse direction by stopped-flow fluorescence energy transfer. The enzyme is preequilibrated with H_4F before the reaction is initiated with $NADP^+$. Final conditions are 3 μM enzyme, 100 μM H_4F, 500 μM $NADP^+$, pH 9, and 25 °C. The theoretical lines represent a single exponential followed by a linear fit.

that the rate of hydride transfer had become too large to measure due to the instrument dead time (1.6 ms). Consequently, at low pH the burst is composed mostly of the dissociation of $NADP^+$. The ability to observe the dissociation of $NADP^+$ in the pre steady state implies that changes in energy transfer are not confined to the chemical reduction step but also occur in the product complexes. For the mutant no isotope-insensitive phase was seen at low pH, suggesting a possible faster dissociation of $NADP^+$ from E–NADP–H_4F ($k_{off} > 1000\ s^{-1}$). A full isotope effect of 3.0 is observed at pH 7.5 (k_{hyd}[NADPH]/k_{hyd}[NADPD] = 520 ± 20 s^{-1}/170 ± 10 s^{-1} = 3.0 ± 0.3).

The rate of hydride transfer in the reverse direction (k_{-hyd}) was measured by fluorescence energy transfer. Typically, 3 μM enzyme was preequilibrated with 100 μM H_4F before 500–1500 μM $NADP^+$ was added. Figure 3 shows a pre-steady-state transient for wild-type mouse DHFR at pH 9. The data were fit to a single exponential of rate 90 ± 10 s^{-1} and a linear rate of 7.1 s^{-1}. Since increasing the pH to 10 or the concentration of $NADP^+$ had no effect on the burst or linear rate, the measured transient was at a pH maximum and was not limited by $NADP^+$ binding. Similar experiments performed on the mutant enzyme gave identical burst values.

Discussion

Binding of Ligands to mDHFR. There are several lines of reasoning which suggest that the binding of NADPH conforms

Scheme IV

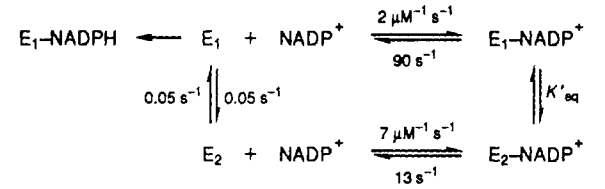

to Scheme I: (1) relaxation binding traces show only one ligand-dependent phase, (2) dissociation rate constants measured by relaxation (Table III) and competition (Table IV) are equivalent, and (3) the ratio of k_{off}/k_{on} is half the measured K_d (Table II). In contrast, the binding requisites outlined in Scheme I are not obeyed by the other ligands. For H_4F two of the criteria are met, although the ratio of k_{off}/k_{on} is 2.1 times the value of K_d. Two explanations can account for this: (1) upon forming an initial collision complex the folate ligand complexes can isomerize to tighter forms, or (2) the ligands can partially bind E_2 in addition to E_1. Although the former has been observed for mutants of *E. coli* DHFR (Adams et al., 1989), the latter may be more likely for reasons that will be considered in the formation of ternary complexes with $NADP^+$ and H_4F.

In the formation of binary complexes with $NADP^+$ there is a clear departure from the simple mechanism of Scheme I. The trapping of preequilibrated mixtures of enzyme and $NADP^+$ with NADPH leads to distinct biphasic kinetics (Table IV). We have interpreted these data as representing the binding of $NADP^+$ to both E_1 and E_2 (Scheme IV).

In this mechanism $NADP^+$ binds E_1 weakly and E_2 tightly. For competition experiments (Table IV), NADPH rapidly traps E_1 at a rate of 90 s^{-1}, with E_2 then slowly isomerizing to E_1 at a rate of 0.05 s^{-1} to completely trap all the enzyme. The relaxation experiments apparently measure the binding of $NADP^+$ to the higher affinity conformation, E_2. The value of k_{on} (3 $\mu M^{-1}\ s^{-1}$) for $NADP^+$ association with E_1 was deduced from the thermodynamic cycle and the K_D for $NADP^+$ (Table II). The correspondence between K_D and k_{off}/k_{on} values results from relatively weak binding of $NADP^+$ to E_1.

This biphasic trapping phenomenon is also present in complexes with both H_4F and $NADP^+$. In the formation of the ternary complexes, the inconsistency of competition and relaxation off rates for the binding of $NADP^+$ to E–H_4F (21 s^{-1} versus 440 s^{-1}) likewise suggests that H_4F binds both E_1 and E_2. To account for this difference we presume that NADPH traps E_1–H_4F and that H_4F, at least, partially binds E_2. The second phase likewise is assigned to isomerization of a second enzyme conformation, in this case E_2–H_4F. It is improbable that either phase results from the reverse reaction (E–N–H_4F → E–NH–H_2F), since the amplitude calculated for such a transient is unobservable in the pre steady state and ligand dependent in the steady state at pH 7. This is further supported by the relaxation data for $NADP^+$ binding to E–H_4F that are similar in value to $NADP^+$ binding to E_2 (Table III). Thus, a mixture of E_1–H_4F and E_2–H_4F prevails under thermodynamic conditions. In addition, since association and dissociation rate constants for $NADP^+$ to E–H_2F are similar to those of the free enzyme (6.8 $\mu M^{-1}\ s^{-1}$ versus 2 $\mu M^{-1}\ s^{-1}$; 13 s^{-1} versus 7 s^{-1}), H_2F also binds E_2 and E_1. However, owing to differences in fluorescent quenching in the various complexes, their equilibrium distribution cannot be estimated.

Since preequilibration with NADPH ensures that E_1 predominates under steady-state cycling, the rate-limiting dissociation of H_4F from the binary complex that controls V_1 (see next section of Discussion) must occur from E_1. The nearly

Scheme V: pH-Independent Kinetic Scheme for Mouse Dihydrofolate Reductase in MTEN Buffer, 25 °C[a]

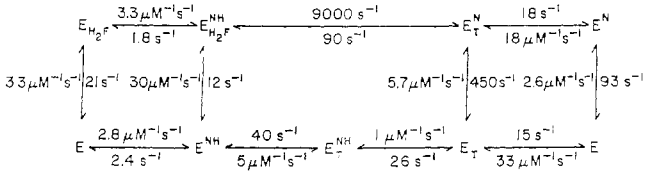

[a] N, $NADP^+$; NH, NADPH; H_2F, dihydrofolate; T, tetrahydrofolate; E, E_1.

coincident values for V_1 (Table I) and k_{off} (Table III) indicate that the relaxation experiments for H_4F binding predominantly measure formation of the E_1 binary complex, E_1–H_4F. By analogy, the binding of H_4F to preequilibrated enzyme and $NADP^+$ forms the ternary complex, E_1–$NADP^+$–H_4F.

Overall Kinetic Scheme for mDHFR. From the data presented under Results and Discussion, it is possible to construct a pH-independent kinetic mechanism for mDHFR. Scheme V outlines the reaction pathway for the conversion of NADPH and H_2F to $NADP^+$ and H_4F as catalyzed by the E_1 conformer of mDHFR. All the association and dissociation rate constants for the ligands to the binary and most ternary complexes have been measured directly by stopped-flow fluorescence spectroscopy. The association rate constants for NADPH to E_1–H_2F and H_2F to E_1–NADPH have been measured under single-turnover conditions (Fierke et al., 1987). The dissociation rate constant for H_2F from the active ternary complex, E_1–NADPH–H_2F, has been estimated by using the coenzyme analogue TNADPH in competition experiments, so that the off rate of NADPH from this active ternary complex has been deduced from the thermodynamic cycle.

The pH-independent rate of hydride transfer in the forward direction was estimated from the pH-dependent burst rates above pH 7.5 and the intrinsic pK_a of Glu-30 as measured by competitive inhibition with DAM. Based on both the errors in the pK_a determination and the observed hydride rates at high pH, the maximum hydride rate is 9000 ± 2000 s^{-1}. At low pH (<7.5) the observed pre-steady-state transients showed no primary deuterium isotope effect. Presumably hydride transfer is too fast to be measured, so that the observed burst is limited mostly by the dissociation of $NADP^+$ from E–NADP–H_4F. This is further supported by the measured dissociation rate constant for $NADP^+$ from E_1–NADP–H_4F of 450 s^{-1} (Table IV). Unlike the case for *E. coli* DHFR (Fierke et al., 1987), NADPH and H_2F dissociation partially control the reverse steady-state rate for mDHFR (Scheme V). Hence, the maximum rate for hydride transfer in the reverse direction was measured from pre-steady-state transients at high pH. The resulting equilibrium for hydride transfer is favorable (K_{int} = 9000 s^{-1}/90 s^{-1} = 100).

Since the dissociation of $NADP^+$ is rapid from the active ternary complex, E–$NADP^+$–H_4F (under normal catalytic cycling no E_2 builds up), the release of H_4F from either E_1–H_4F (at low NADPH) or E_1–NADPH–H_4F (at high NADPH) is rate determining for V_1 or V_2, respectively. Although k_{off} from E_1–H_4F could be independently measured in the stopped-flow instrument, k_{off} from the ternary complex could not. Hence, V_2 is assumed to be limited by the NADPH-assisted off rate of H_4F from E–NADPH–H_4F. Kinetic simulations of Scheme V using KINSIM indicate that a dissociation rate constant of 40 s^{-1} is required to account for the experimental value of V_2. Thus, the binding of NADPH to E–H_4F accelerates the dissociation rate of H_4F almost 3-fold (15 s^{-1} versus 40 s^{-1}). This negative synergism between NADPH and H_4F is general for all DHFRs studied (Fierke et al., 1987; Andrews et al., 1989) and is contrasted strongly by the lack of synergism observed between NADPH and H_2F.

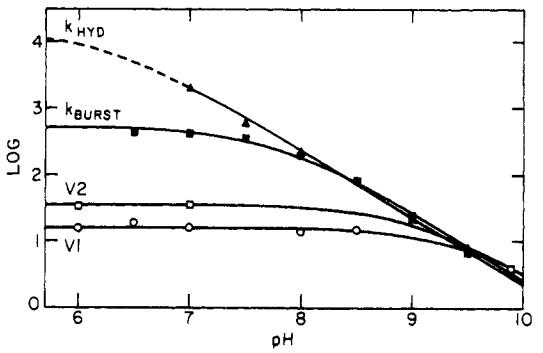

FIGURE 4: Variation of the maximal steady-state parameters, V_1 (○) and V_2 (□), the observed burst rate, k_{obs} (■), and the observed hydride transfer rate, k_{hyd} (▲), as a function of pH for mDHFR at 25 °C, MTEN buffer. The solid lines for k_{obs} and k_{hyd} are based on maximum rates of 540 s^{-1} and 9000 s^{-1}, respectively. The dashed line indicates that the hydride transfer rate under these pH conditions could not be directly measured but only inferred from the pK_a of Glu-30 (see Discussion). The solid lines for V_1 and V_2 were generated from Table I.

Scheme VI

$$\text{E–NH–H}_2\text{F} + \text{H} \underset{K_a}{\rightleftharpoons} \text{H–E–NH–H}_2\text{F} \underset{k_{-hyd}}{\overset{k_{hyd}}{\rightleftharpoons}} \text{E–N–H}_4\text{F} \xrightarrow{k_{diss}}$$

The pH dependence of the above mechanism (Scheme V) is illustrated in Scheme VI. An acidic residue (Glu-30) with a pK_a of 6.4 is responsible not only for the attenuation of V but also for that in the hydride transfer step. The net effect is that the pK_a's in both V_1 and V_2 are perturbed upward from 6.4. Thus, the steady-state and transient kinetic parameters are described by a change in rate-determining step from either H_4F or $NADP^+$ dissociation at low pH to hydride transfer at high pH. This interdependence of hydride transfer, H_4F dissociation, and V is illustrated in Figure 4.

To test the validity of Schemes V and VI, the kinetic simulation program KINSIM was used to predict all the initial velocity and full time-course kinetics. Table I enumerates all the experimentally determined steady-state parameters as well as some of the observed isotope effects. Schemes V and VI were capable of predicting these values to within an acceptable error. The congruency of predicted and experimental values for some of the steady-state parameters is shown in Table V. Scheme V was also able to predict full time-course kinetics for the net conversion of substrates to products at various concentrations of NADPH and H_2F (Figure 5). A third check on Scheme V was made by showing that the internal equilibrium constant for hydride transfer (K_{int} = 100) could be scaled to the overall equilibrium constant for the net pH-independent conversion of substrates to products. Scheme VII represents the overall, abridged mechanism where $K_{ov} = K_{int}(1/K_a)(K_4/K_2)$. For Scheme VII K_{ov} has been calculated to be 2.6 × 10^{10} M^{-1}, which agrees well with the experimentally determined value of 6.5 (±4) × 10^{10} M^{-1} (Fierke et al., 1987).

Scheme VII

$$\text{E} + \text{H} \underset{K_a}{\rightleftharpoons} \text{H–E} + \text{NH} + \text{H}_2\text{F} \underset{K_2}{\rightleftharpoons} \text{H–E–NH–H}_2\text{F} \overset{K_{int}}{\rightleftharpoons}$$

$$\text{E–N–H}_4\text{F} \overset{K_4}{\rightleftharpoons} \text{E} + \text{N} + \text{H}_4\text{F}$$

Table V: Predicted Steady-State Parameters for mDHFR[a]

	predicted	measured
100 μM NADPH, 1–100 μM H_2F, pH 7		
V_M (s^{-1})	27	28 ± 2
K_M (μM)	0.75	0.9 ± 0.3
50 μM H_2F, 0.5–800 μM NADPH		
V_1 (s^{-1})	18	17 ± 2
K_1 (μM)	6.5	6.2 ± 1
pK_a	9.2	9.36 ± 0.06
V_2 (s^{-1})	36	36 ± 2
K_2 (μM)	40	49 ± 4
pK_a	8.8	9.15 ± 0.07
k^H/k^D (pH 9)	1.8	1.71 ± 0.05
k^H/k^D (pH 10)	2.8	3.3 ± 0.25
280 μM H_4F, 840 μM $NADP^+$		
V (s^{-1}) (pH 10)	7.9	7.2 ± 0.9
pK_a (V)	8.2	8.10 ± 0.09

[a] MTEN buffer, 25 °C.

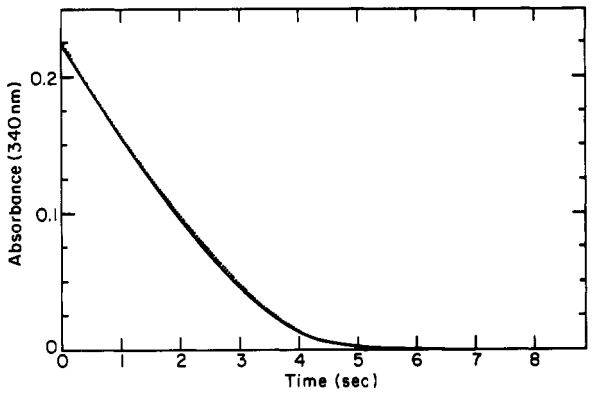

FIGURE 5: Full time-course kinetics as measured by stopped-flow absorbance. mDHFR is preincubated with NADPH and the reaction is initiated with H_2F. Final conditions are 0.17 μM enzyme, 100 μM NADPH, 10 μM H_2F, pH 7.0, 25 °C, and MTEN buffer. The curve was simulated by the program KINSIM according to Scheme V. The ordinate axis represents the time-dependent absorbance minus the equilibrium value ($A_t - A_{eq}$).

Folate Reduction for mDHFR. In addition to the facile reduction of H_2F, mDHFR can catalyze the slower reduction of folic acid to H_4F. Since the former reduction is fast and H_2F and $NADP^+$ can rapidly dissociate from the enzyme, the rates observed for the reduction of folic acid are solely limited by chemistry. Although the observed rate of this reduction increases with decreasing pH, there is no plateau region as low as pH 5 despite the measured pK_a of 6.4 for Glu-30. The simplest interpretation is that Glu-30 is not involved in pterin protonation. The role of Glu-30 for folic acid reduction may be only to position the pterin ring via hydrogen bonding, with direct protonation by solvent. This phenomenon has been observed for several mutants of *E. coli* DHFR that have removed the donating capacity of Asp-27 by replacement with Asn and Ser (Howell et al., 1986). For these mutants V increases indefinitely with increasing pH, indicating solvent protonation in dihydrofolate reduction.

Effects of Salt on Binding and Catalysis. Since the complete elucidation of the kinetic mechanism for mDHFR was facilitated by salt concentrations higher than those used for the *E. coli* enzyme (see Results), we probed the specific effects of NaCl on the binding of substrates and products and the rates of hydride transfer. Overall, buffers containing low salt show binding enhancements ranging from 1.8 kcal/mol for folic acid to 3.1 kcal/mol for NADPH. Relaxation experiments performed at the lower salt concentrations indicate that as much as 50% of the ground-state stabilization of the enzyme–ligand complexes can be attributed to an increase in k_{on}.

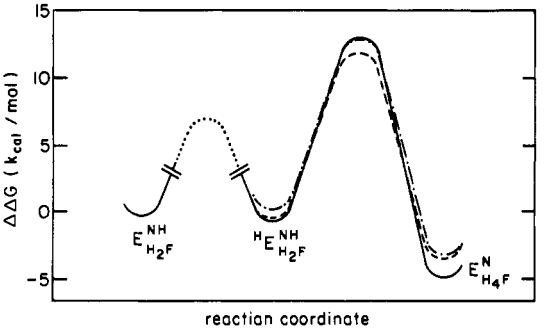

FIGURE 6: Gibbs free energy coordinate diagram for mouse (—), *E. coli* (- - -), and *L. casei* (- · -) dihydrofolate reductases aligned at the protonated substrate ternary complex, H–E–NH–H_2F, pH 7.0, and 25 °C.

Since ligand binding is sensitive to salt, we questioned whether these effects would be manifested in the internal enzyme mechanism (i.e., the forward and reverse rates of hydride transfer for both H_2F and folic acid and the pK_a of Glu-30). Kinetic measurements of folate reduction at various pHs at 0.1 M NaCl were found to be identical with those at 0.8 M NaCl (data not shown). In addition, the pK_a of Glu-30 is only mildly sensitive to salt (6.4 versus 7.0 ± 0.1). Since the effect on Glu-30 is small, the maximum hydride transfer rate is unaffected by salt. Furthermore, the magnitude of pre-steady-state transients in the reverse direction with saturating concentrations of $NADP^+$ and H_4F are salt independent, so that the internal equilibrium constant is approximately unchanged (K_{int} = 100). The salt insensitivity of key kinetic steps permits the comparison of both wild-type and mutant mDHFRs to the *E. coli* and *L. casei* enzymes (Figure 6). Despite considerable primary sequence differences at the three active sites, key elements—the internal chemical equilibrium, the pK_a of the active-site acid, and the rate of hydride transfer—are energetically similar and differ by no more than 1 kcal/mol.

Comparison of Wild-Type and Mutant mDHFRs. The H_2F binding sites of all known DHFRs are primarily composed of hydrophobic amino acids, particularly in the region of the pterin and benzoyl rings. Despite this stringent network of residues, there is only one ionizable group in contact with the pterin ring. In all known bacterial and mammalian DHFRs this group is the carboxyl of either aspartic acid or glutamic acid, in that order. In both cases, the carboxyl is nearly coplanar with the pterin heterocycle, making either direct or indirect hydrogen-bonding contacts (Bolin et al., 1982; Oefner et al., 1988). It is conjectured that proton transfer occurs from the carboxyl to the N5 via proximal water molecules and not through a direct transfer owing to its relative position (Gready, 1985). Nevertheless, the ability of mammalian DHFRs to efficiently reduce folic acid compared to the bacterial enzymes may rest in the selection of the active-site proton donor. To this end we have studied the effects of substituting aspartic acid for glutamic acid at position 30 in mDHFR.

Despite the positioning of Glu-30 in the active site, the deletion of a methylene group has little or no effect on the dissociation constants of all ligands tested (Table II). Consequently, the steady-state parameters and observed isotope effects for the mutant are similar in value to those for the wild-type enzyme (Table I). The maximal velocities, V_1 and V_2, are comparable to those of wild type, suggesting that H_4F dissociation is only moderately affected but still rate limiting at low pH. The maximum rate of hydride transfer to H_2F was estimated from the intrinsic pK_a of Asp-30. Since the pK_a in the mutant is 6.0 and the observed rates of hydride transfer

are the same as in wild type above pH 7.5, the maximum hydride transfer rate is calculated to be 20000 ± 6000 s^{-1}. Although this value is approximately 2-fold higher than for wild type, the reverse rate of hydride transfer is unaffected so that the internal equilibrium constant is only slightly changed (K_{eq} = 200). Hence, the overall effects of the mutation on the binding of ligands and the delivery of both a proton and a hydride ion to H_2F are diminutive. This indicates that the addition of a single methylene has little effect on the net conversion of H_2F to H_4F.

In contrast to the effects on H_2F reduction, the rate of folic acid reduction is markedly decreased 10-fold in the mutant, although the hydride transfer step is entirely rate limiting. However, the larger isotope effects observed for the mutant relative to wild type (Table I) indicate that the transition state for folic acid reduction may be more symmetrical. Nevertheless, the pH sensitivity of V is nearly identical with that of the wild type, suggesting solvent participation in the proton transfer step as observed in wild type. The rates of folic acid reduction at pH 6 for *E. coli* and *L. casei* DHFRs have been determined to be 0.0027 s^{-1} (R. Bethell, personal communication, 1989) and 0.066 s^{-1} (Andrews et al., 1989), respectively. This compares with 0.44 s^{-1} (Table I) for the mouse enzyme at the same pH. Hence, the lower reduction rate observed for the mutant (0.06 s^{-1}; Table I) suggests that a single replacement can confer the observed species specificity. Whether mutation of the active-site aspartic acid to glutamic acid in both bacterial sources leads to a rate enhancement for folate reduction similar to that observed in the mouse enzyme remains to be seen.

Acknowledgments

We thank Kaye Yarnell for the diligent typing of the manuscript.

References

Adams, J., Johnson, K. A., Matthews, R., & Benkovic, S. J. (1989) *Biochemistry 28*, 6611–6618.

Andrews, J., Fierke, C. A., Birdsall, B., Ostler, G., Feeney, J., Roberts, G. C. K., & Benkovic, S. J. (1989) *Biochemistry 28*, 5743–5750.

Barshop, B. A., Wrenn, R. F., & Frieden, C. (1983) *Anal. Biochem. 130*, 134–145.

Birdsall, B., Burgen, A. S. V., & Roberts, G. C. K. (1980) *Biochemistry 19*, 3723–3731.

Blakley, R. L. (1960) *Nature (London) 188*, 231–232.

Bolin, J. T., Filman, D. J., Matthews, D. A., Hamlin, R. C., & Kraut, J. (1982) *J. Biol. Chem. 257*, 13650–13662.

Brown, D. J., & Jacobsen, N. W. (1961) *J. Chem. Soc.*, 4413–4420.

Cayley, P. J., Dunn, S. M. J., & King, R. W. (1981) *Biochemistry 20*, 874–879.

Curthoys, H. P., Scott, J. M., & Rabinowitz, J. C. (1972) *J. Biol. Chem. 247*, 1959–1964.

Dawson, R. M. C., Elliott, D. C., Elliott, W. H., & Jones, K. M. (1969) in *Data for Biochemical Research*, Oxford University Press, Oxford, England.

Dunn, S. M. J., & King, R. W. (1980) *Biochemistry 19*, 766–773.

Dunn, S. M. J., Batchelor, J. G., & King, R. W. (1978) *Biochemistry 17*, 2356–2364.

Dyson, R. D., & Isenberg, I. (1971) *Biochemistry 10*, 3233–3241.

Fierke, C. A., Johnson, K. A., & Benkovic, S. J. (1987) *Biochemistry 26*, 4085–4092.

Gready, J. E. (1985) *Biochemistry 24*, 4761–4766.

Howell, E. E., Villafranca, J. E., Warren, M. S., Oatley, S. J., & Kraut, J. (1986) *Science (Washington, D.C.) 231*, 1123–1128.

Howell, E. E., Warren, M. S., Booth, C. L. J., Villafranca, J. E., & Kraut, J. (1987) *Biochemistry 26*, 8581–8598.

Johnson, K. A. (1986) *Methods Enzymol. 134*, 677–705.

Kallen, R. G., & Jencks, W. P. (1966) *J. Biol. Chem. 241*, 5845–5850.

Matthews, C. K., & Huennekens, F. M. (1960) *J. Biol. Chem. 235*, 3304–3308.

Matthews, D. A., Bolin, T. J., Burridge, J. M., Filman, D. J., Volz, K. W., Kaufman, B. T., Beddel, C. R., Champness, J. N., Stammers, D. K., & Kraut, J. (1985) *J. Biol. Chem. 260*, 381–391.

Oefner, C., D'Arcy, A., & Winkler, F. K. (1988) *FEBS Lett. 237*, 377–385.

Rabinowitz, J. C. (1960) in *The Enzymes*, 2nd ed. (Boyer, P. D., Lardy, H., & Myrbaeck, K., Eds.) Vol. 2, pp 185–252, Academic Press, New York.

Seeger, D. R., Cosulick, D. B., Smith, J. M., & Hultquist, M. E. (1949) *J. Am. Chem. Soc. 71*, 1753–1758.

Segel, I. H. (1975) in *Enzyme Kinetics, Behavior and Analysis of Rapid Equilibrium and Steady-State Enzyme Systems*, p 109, Wiley, New York.

Stammers, D. K., Champness, J. N., Beddel, C. R., Dann, J. G., Eliopoulos, E., Geddes, A. J., Ogg, D., & North, A. C. T. (1987) *FEBS Lett. 218*, 178–184.

Stone, S. R., & Morrison, J. F. (1983) *Biochim. Biophys. Acta 745*, 247–258.

Taira, K., & Benkovic, S. J. (1988) *J. Med. Chem. 31*, 129–137.

Thillet, J., Absil, J., Stone, S. R., & Pictet, R. (1988) *J. Biol. Chem. 263*, 12500–12508.

Viola, R. E., Cooke, P. F., & Cleland, W. W. (1979) *Anal. Biochem. 96*, 334–340.

Volz, K. W., Matthews, D. A., Alden, R. A., Freer, S. T., Hansch, C., Kaufman, B. T., & Kraut, J. (1982) *J. Biol. Chem. 257*, 2528–2536.